SI APPENDIX

Pyridoxal Kinase Inhibition by Artemisinins Downregulates Inhibitory Neurotransmission

Vikram Babu Kasaragod[1,4,5,*], Anabel Pacios-Michelena[1,4], Natascha Schaefer[2], Fang Zheng[3], Nicole Bader[1], Christian Alzheimer[3], Carmen Villmann[2] and Hermann Schindelin[1,*].

www.pnas.org/cgi/doi/10.1073/pnas.2008695117

Figure S1

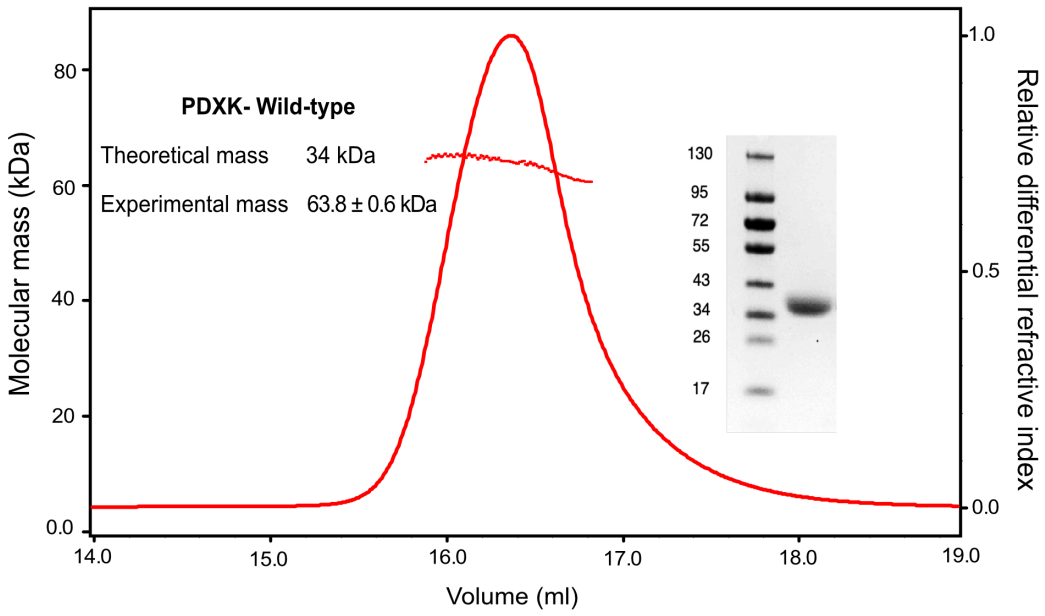

Figure S1. MALS measurements of WT PDXK. Multi angle laser light scattering coupled to size exclusion chromatography (SEC-MALS) of recombinantly expressed and purified WT-PDXK along with an SDS-PAGE analysis of the purified protein (inset). The normalized differential refractive index is represented along with the measured molecular mass under the curve. The experimental derived mass of 63.8 kDa demonstrates that the protein forms a dimer in solution considering a calculated monomer weight of 34 kDa.

Figure S2

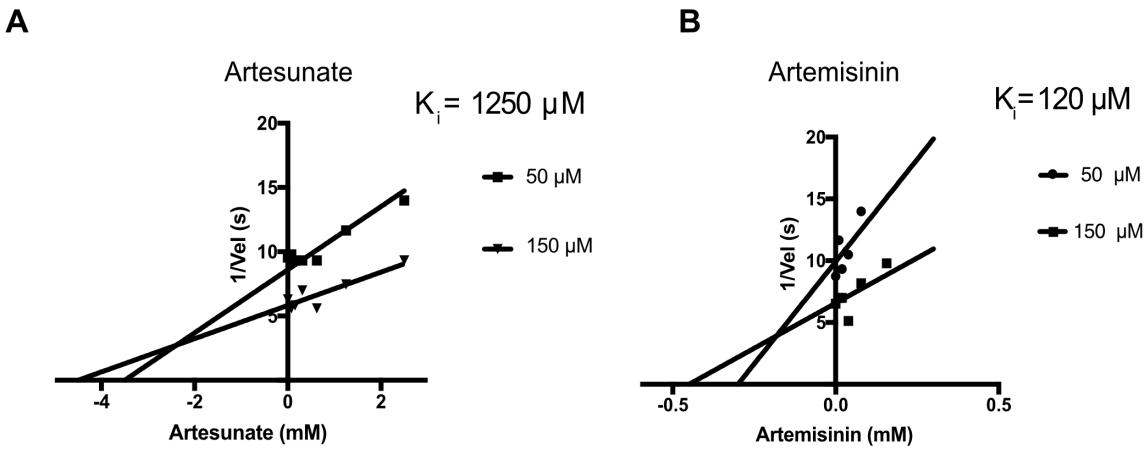

Figure S2. Inhibition analysis. (A-B) Dixon plots for the inhibition of PDXK by artesunate **(A)** and artemisinin **(B).** The succinate derivative of artemisinin displays a K_i of 1250 µM in contrast to the more potent artemisinin with a K_i of 120 µM.

Figure S3

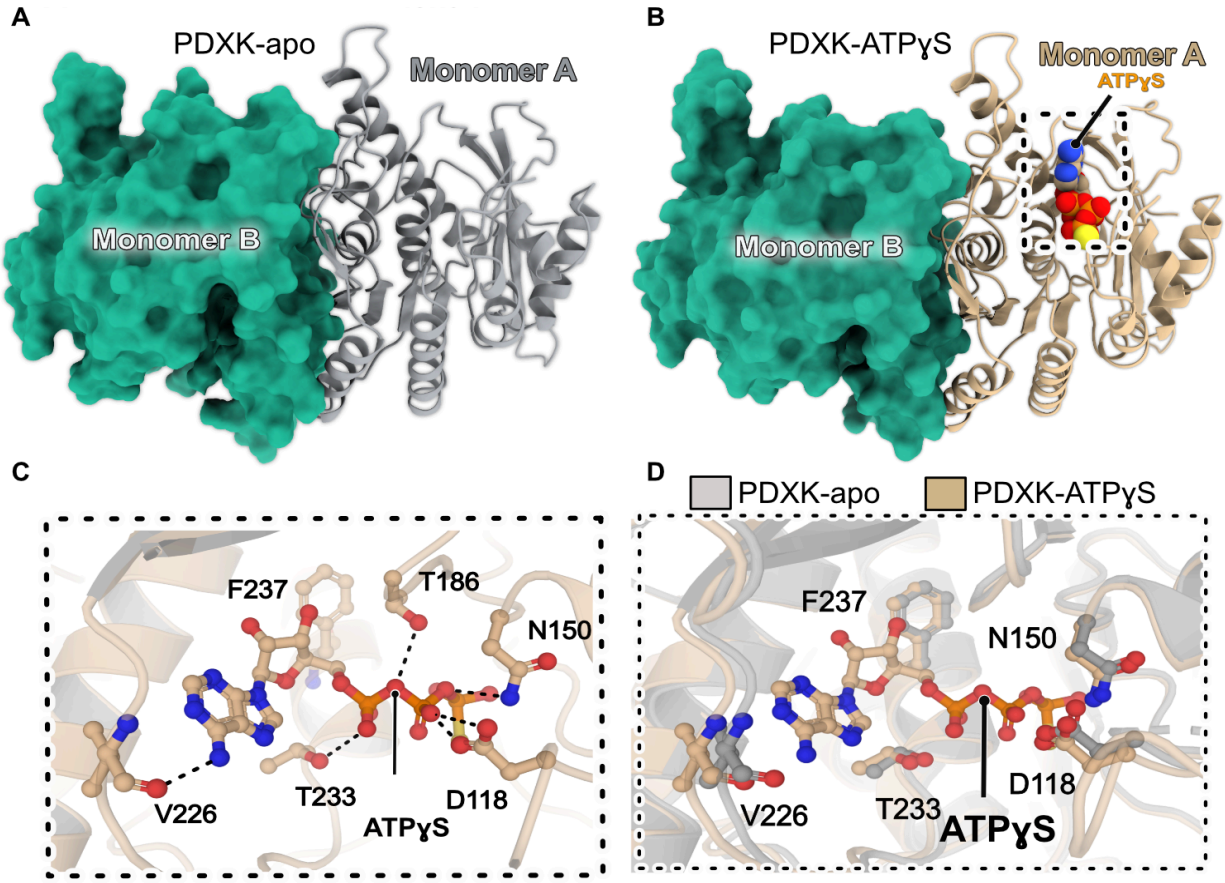

Figure S3. Structural comparison of apo-PDXK and the PDXK-ATPγS complex.

(A-B) Overall architecture of apo-PDXK (A) and the PDXK-ATPγS (B) complex. One protomer is shown in cartoon and the second in surface representation. ATPγS is displayed in CPK representation.

(C) Enlarged view of the ATPγS binding pocket. The ligand and residues crucial for binding are shown in ball and stick representation and the protein backbone as a cartoon.

(D) Comparative analyses of the PDXK-apo and PDXK-ATPγS structures. One monomer of PDXK-apo and PDXK-ATPγS are displayed in gray and brown cartoon representation, respectively.

Figure S4

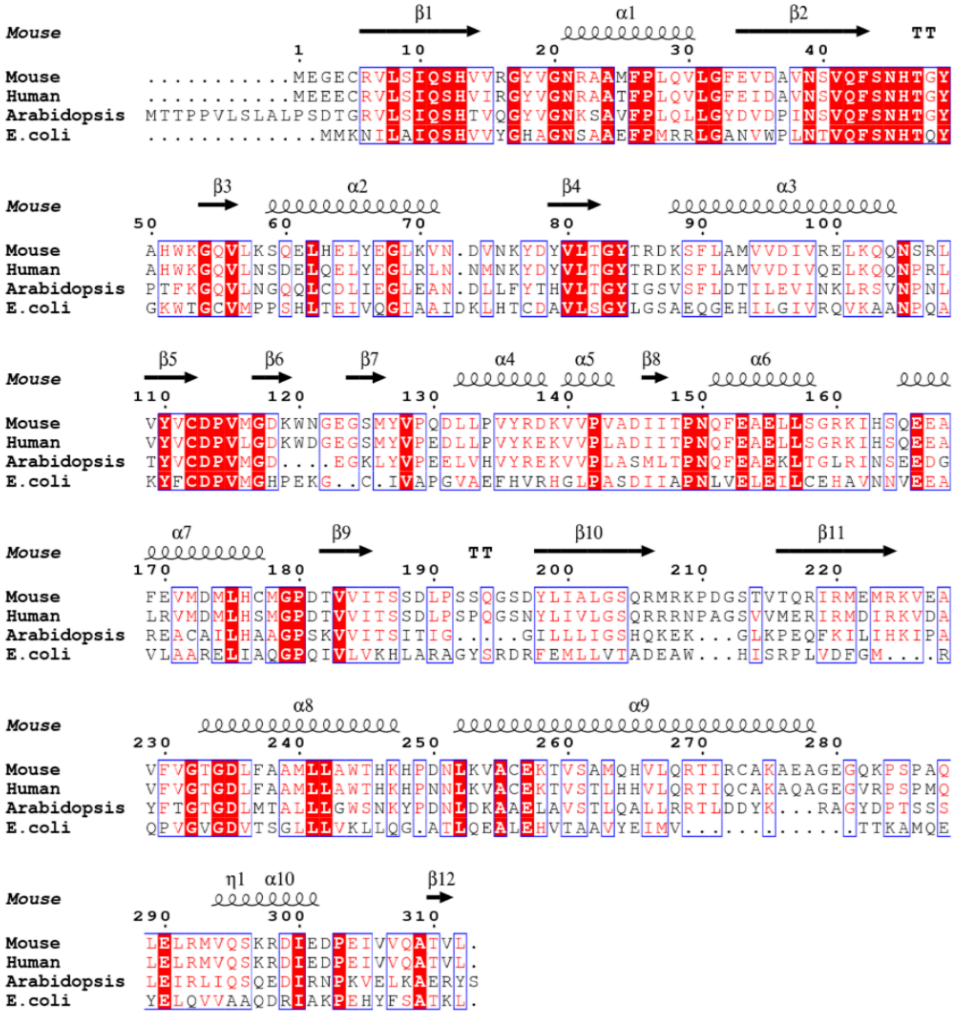

Figure S4. Multiple sequence alignment. Multiple sequence alignment of PDXK enzymes from diverse sources obtained with Clustal omega (1) and represented by using the ESPript server (2).

Figure S5

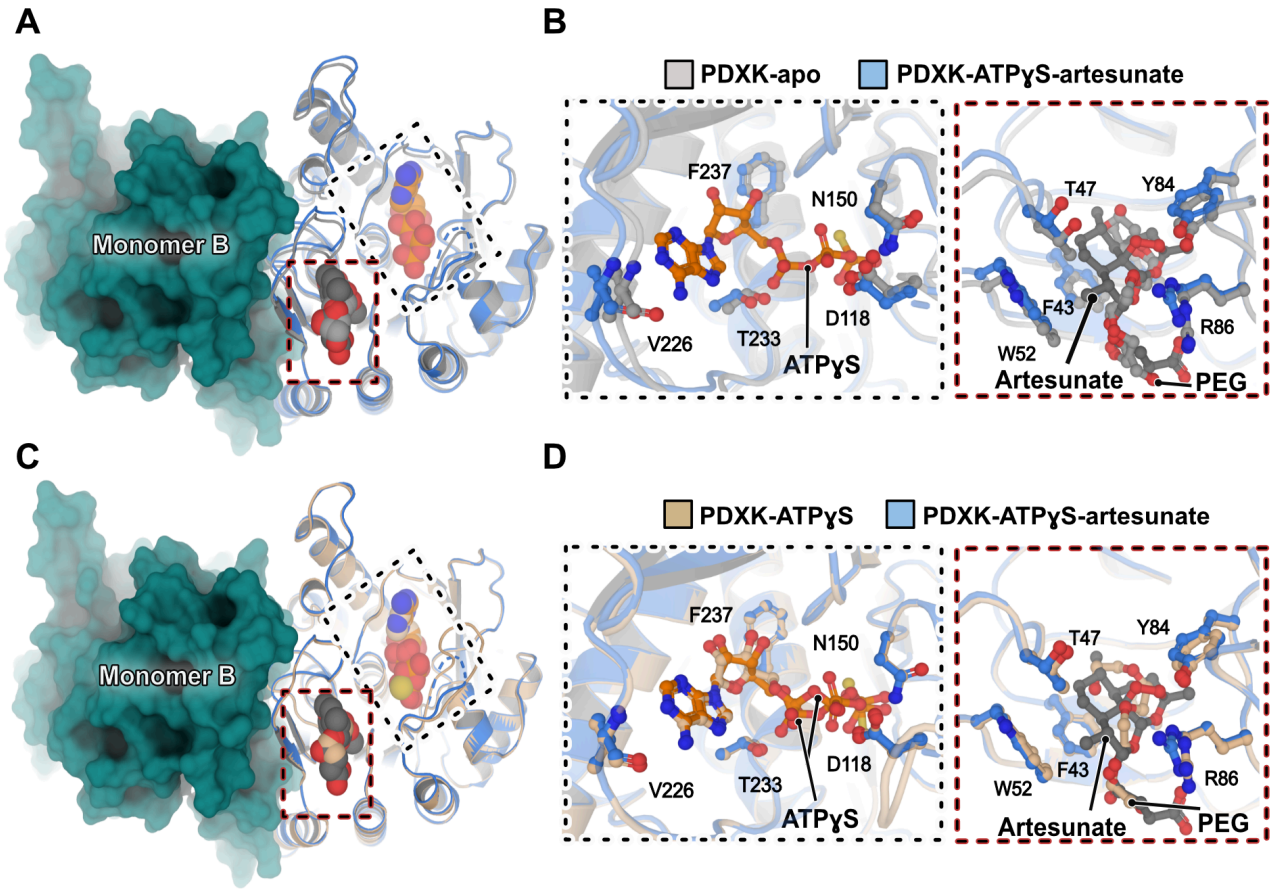

Figure S5. Structural comparison of the apo, the PDXK-ATPγS and the PDXK-ATPγS-artesunate structures.

(A-B) Comparison of the PDXK-ATPγS-artesunate structure with the apo structure. The overall architecture is shown in **(A)** and enlarged views of the ligand binding pocket are shown in **(B)**.

(C-D) Comparison of the ternary PDXK-ATPγS-artesunate and binary PDXK-ATPγS complexes. The overall architecture is shown in **(C)** and enlarged views of the ligand binding pocket are shown in **(D)**. In panels **B** and **D**, bound ligands and residues, which are crucial for binding, are shown in ball and stick representation and the protein backbone in cartoon representation. Please note that in the apo and in the binary PDXK-ATPγS structure, the

artemisinin binding pocket is occupied by polyethylene glycol, a component of the crystallization solution.

Figure S6

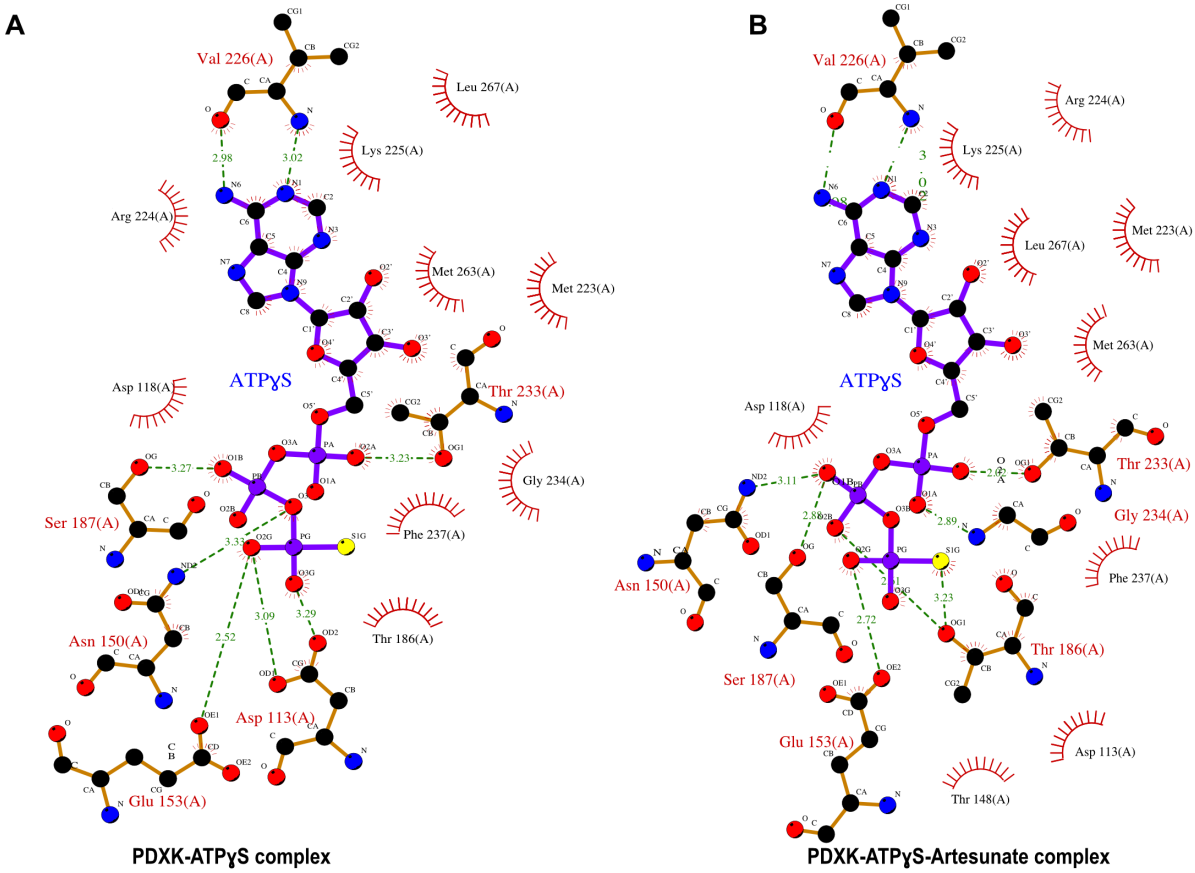

Figure S6. Comparison of ATP binding pockets in the binary and ternary complexes.

(A-B) LigPlot 2D-representation of ATPγS from the binary PDXK-ATPγS **(A)** and ternary PDXK-ATPγS-artesunate **(B)** complexes derived from an analysis with the ProFunc server (3). Please note that residues mediating the binding of ATPγS are almost identical in both structures as is the conformation of the bound ATPγS (not shown).

Figure S7

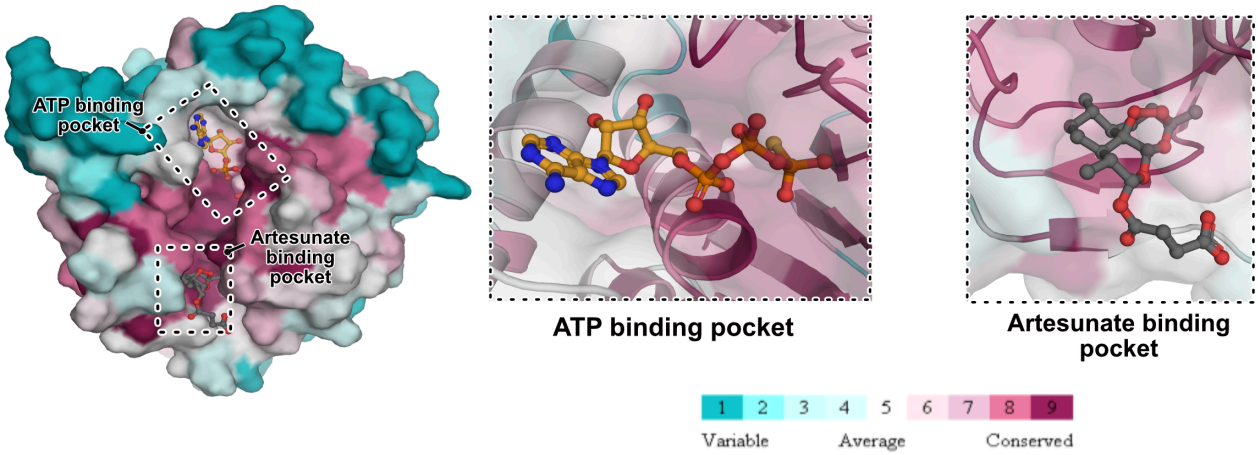

Figure S7. Sequence conservation analysis. PDXK sequence conservation analyzed with the ConSurf server (4). Overall architecture of a PDXK monomer colored according to the accompanying conservation scores (see scale below). Enlarged views of the ATP and the artesunate binding pockets clearly show that both binding pockets are evolutionarily highly conserved.

Figure S8

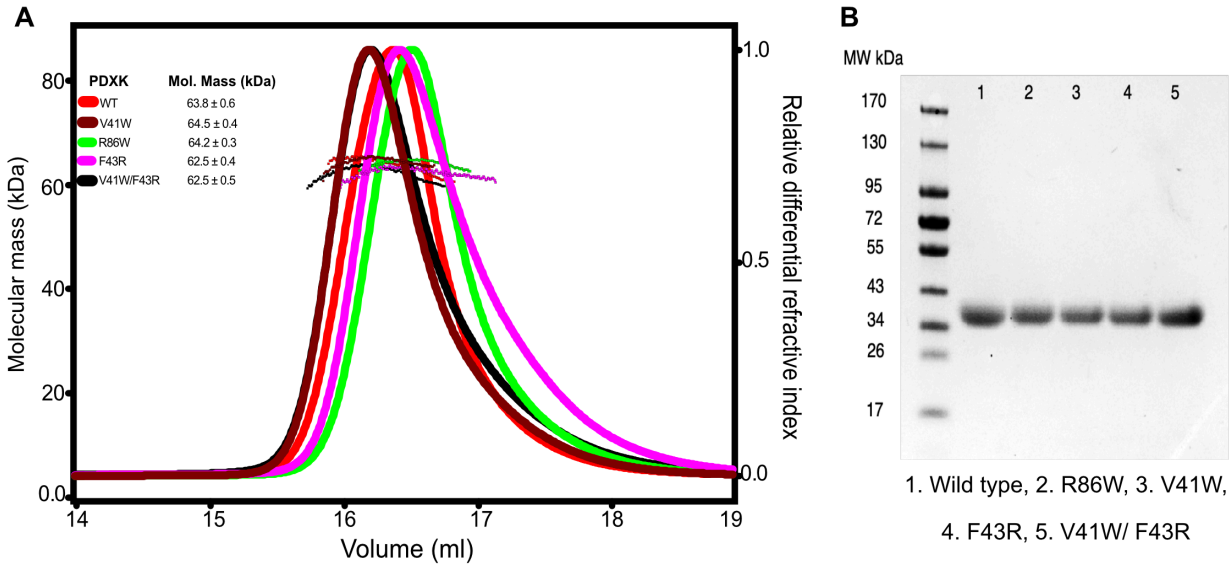

Figure S8. Biophysical and biochemical analysis of PDXK variants.

(A) SEC-MALS analyses of the wildtype and PDXK mutants. The data confirm that, like the wild-type protein, all mutants dimerize. Please note that due to non-synchronized injections the elution volumes of the different samples are slightly offset.

(B) SDS-PAGE analysis of purified PDXK variants and the wild-type.

Figure S9

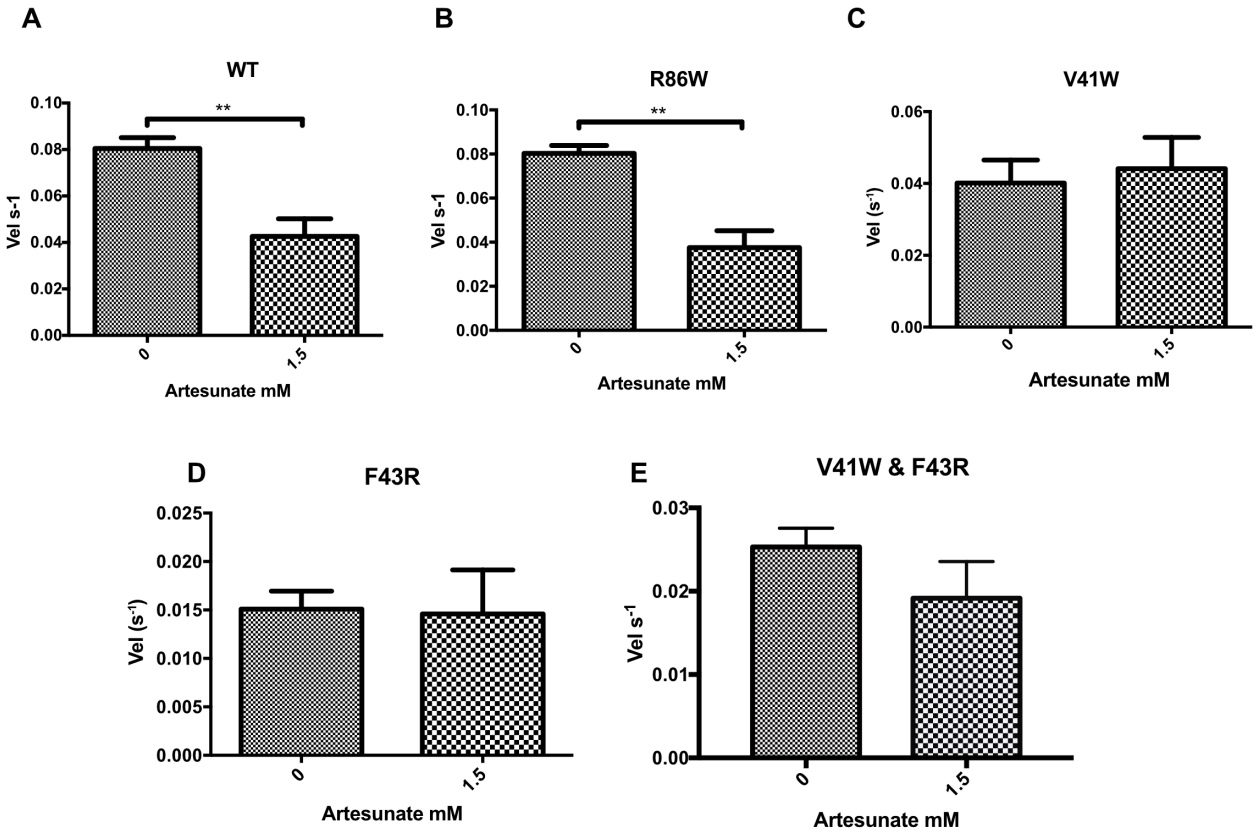

Figure S9. Inhibition analysis of PDXK variants.

(A-E) Bar diagrams of the turnover rates of PDXK variants in the absence and presence of artesunate (1.5 mM). Please note that R86W **(B)** behaves similar as the WT **(A)** with artesunate retaining its inhibition potency, whereas the variants V41W **(C),** F43R **(D)** and the double mutant V41W/F43R **(E)** completely abolish artesunate binding. Data are presented as mean ± SEM (p values are: *p<0.05; **p<0.01; ***p<0.001; ****p<0.0001, Paired *t* test).

Figure S10

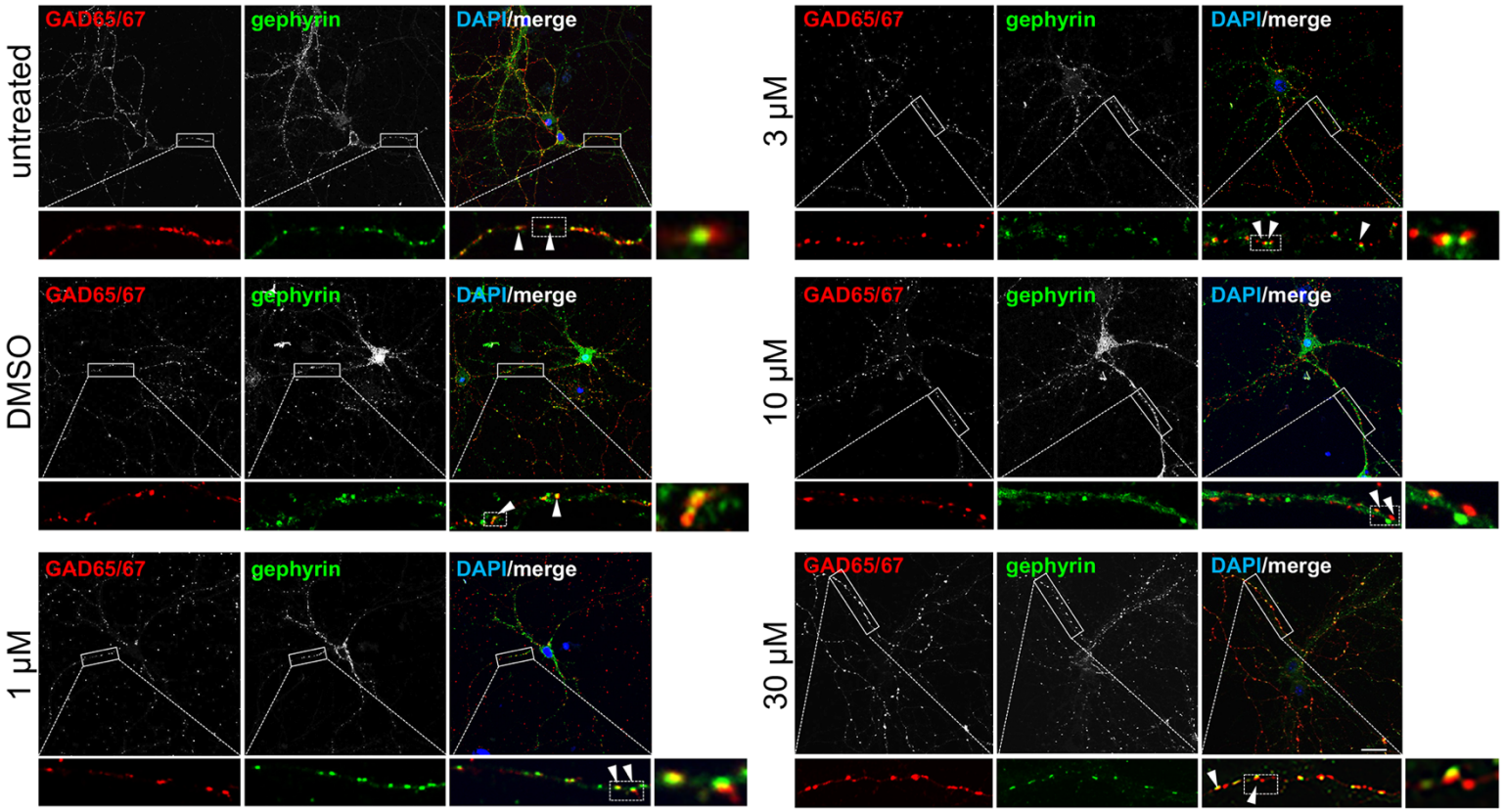

Figure S10. Artemisinins do not change the expression levels of GAD. Immunocytochemical staining of hippocampal neurons were performed at DIV14. Untreated cells, DMSO treated controls, and artemisinin (1, 3, 10, 30 µM) treated cells are shown. Cells were stained for GAD65/67 (red, shown in white), gephyrin (green, shown in white), and with DAPI (blue) to label the nucleus. The merge of all channels is presented in the right panels (yellow color indicates a colocalization of GAD65/67 and gephyrin). The white scale bar (lower right) refers to 50 µm. The white box marks a dendrite, which is enlarged below each image. Enlarged views of individual synaptic boutons (enclosed by white dotted boxes) representing presynaptic (GAD65/67) and postsynaptic (Geph) are shown on the right and predominantly reveal apposition of the two proteins.

Figure S11

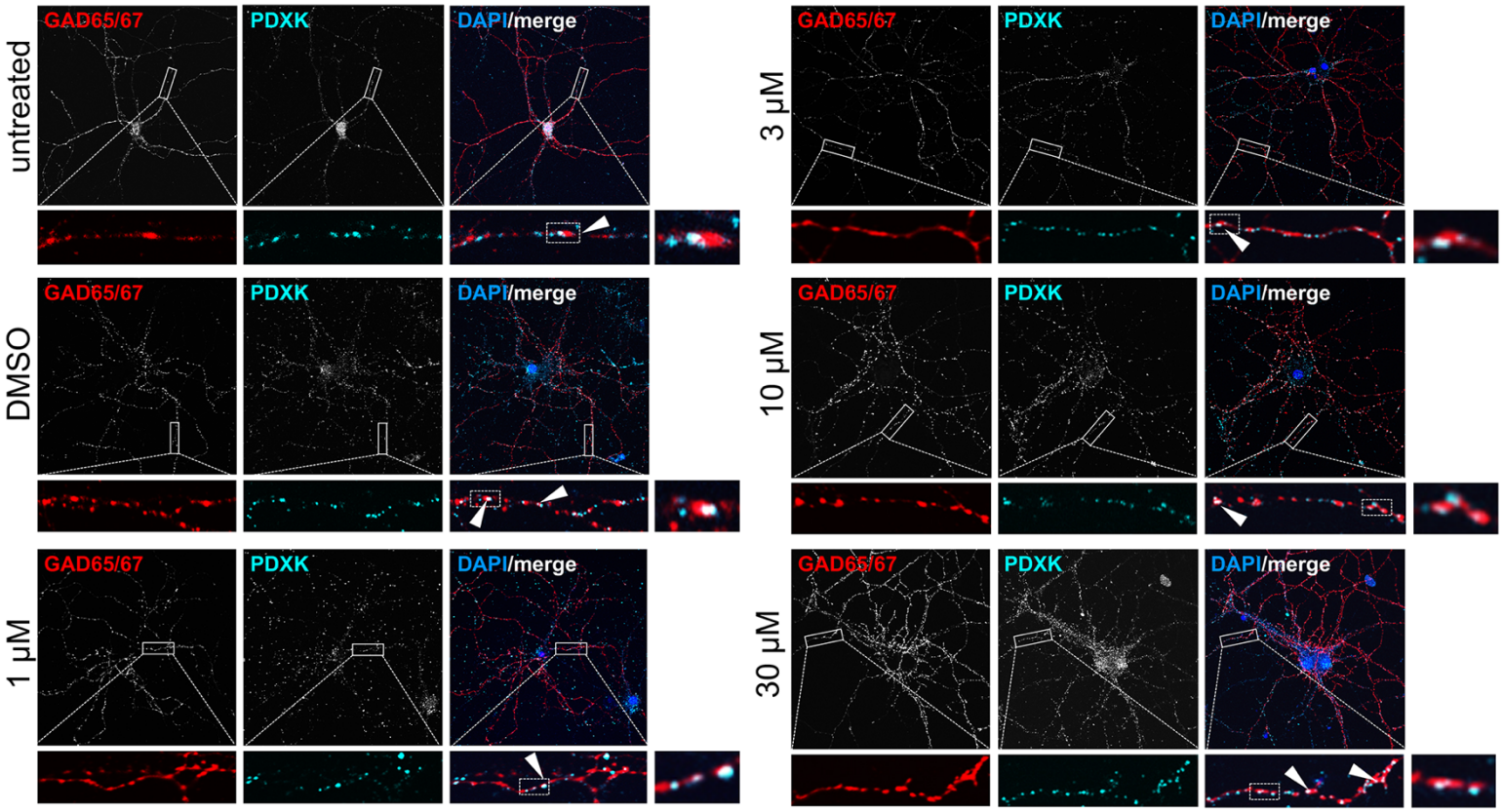

Figure S11. Artemisinins do not lead to obvious changes in the whole cell expression of PDXK. Hippocampal neurons at DIV14 were stained for GAD65/67 (red, shown in white), PDXK (cyan, shown in white), and DAPI (blue) to label the nucleus. The merge of all channels is presented in the right panels. Untreated cells, DMSO treated controls, and artemisinin (1, 3, 10, and 30 µM) treated cells are shown. Note, no change in GAD and PDXK intensity was observed between different conditions. The white box labels a dendrite shown in the image below (enlarged images). Enlarged views of individual synaptic boutons (white dotted box) representing GAD65/67-red and PDXK-cyan are presented to the right of the dendritic images. White arrow heads point to colocalization of GAD65/67 and PDXK.

Figure S12

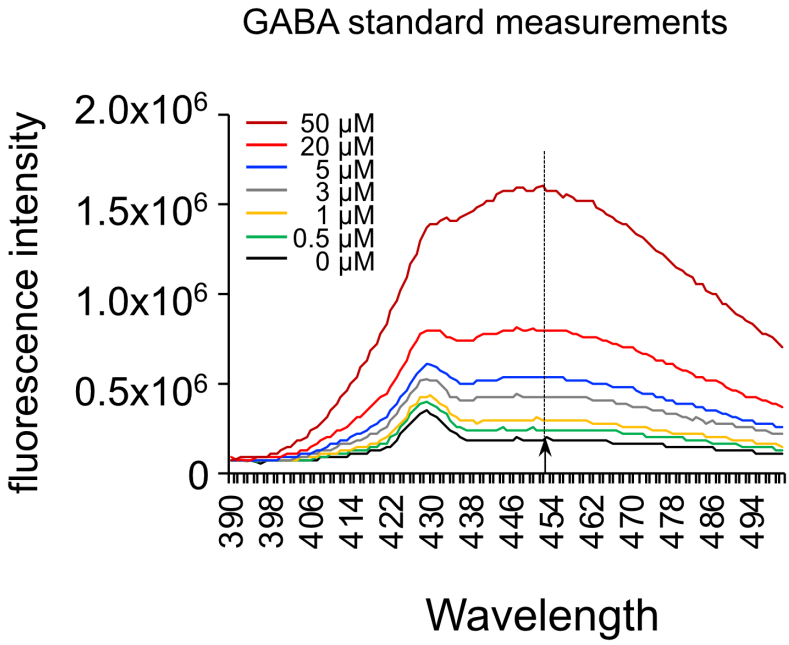

Figure S12. GABA standard measurements. A concentration series of GABA was established (0, 0.5, 1, 3, 5, 20, 50 µM) by measuring the fluorescence spectrum from 390 to 500 nm. GAD activity was quantified based on the emission at 450 nm (marked by an arrow and a dotted line). These standard values were used to measure the amount of GABA synthesized by GAD as shown in **Fig. 5D**.

Reference:

1. F. Sievers *et al.*, Fast, scalable generation of high-quality protein multiple sequence alignments using Clustal Omega. *Mol Syst Biol* **7**, 539 (2011).
2. X. Robert, P. Gouet, Deciphering key features in protein structures with the new ENDscript server. *Nucleic Acids Res* **42**, W320-324 (2014).
3. R. A. Laskowski, J. D. Watson, J. M. Thornton, ProFunc: a server for predicting protein function from 3D structure. *Nucleic Acids Res* **33**, W89-93 (2005).
4. H. Ashkenazy *et al.*, ConSurf 2016: an improved methodology to estimate and visualize evolutionary conservation in macromolecules. *Nucleic Acids Res* **44**, W344-350 (2016).